Supplementary Information

Developing $Fe_xCo_yLa_z$-based amorphous aerogel catalyst for oxygen evolution reaction via high throughput synthesis

Bijun Cai[#,1], Shaomeng Xu[#,1,3], Zhuyang Chen[,1] Weixuan Li[1], Ronggui Zhu[1,2], Shibo Xi[4], Chen Xu*[,2], and X.-D. Xiang*[,1,2]*

1. School of Materials Science and Engineering,
Southern University of Science and Technology, 1088 Xueyuan Avenue, Shenzhen 518055, P.R. China
2. Academy for Advanced Interdisciplinary Studies,
Southern University of Science and Technology, 1088 Xueyuan Avenue, Shenzhen 518055, P.R. China
3. School of Materials Science and Engineering, Harbin Institute of Technology, Harbin 150001, P.R. China
4. Institute of Chemical and Engineering Sciences, A*STAR (Agency for Science, Technology and Research), 1 Pesek Road, Jurong Island, Singapore 627833, Singapore

E-mail: xuc3@sustech.edu.cn, chenzy3@sustech.edu.cn, xiangxd@sustech.edu.cn

Video S1. (Supplementary Video 1) High throughput fabrication for amorphous aerogel catalyst.

Preset Ratio			The mass fraction of each element in the aerogel				Actual Element Ratio					
Fe	Co	La	Fe (wt%)	Co (wt%)	La (wt%)	Total(wt%)	Fe(at%)	Co(at%)	La(at%)	Atom Ratio		
2	3	3	8.6	13.2	29.7	51.4	25.8	37.6	36.6	2.2	3.1	3.1
2	4	2	10.1	24.0	26.4	60.4	23.2	52.1	24.7	1.9	4.2	2.0
3	3	2	8.6	5.6	16.6	30.8	40.5	27.0	32.4	3	2	2.4
3	2	3	10.5	8.2	30.1	48.8	34.4	25.4	40.2	2.9	2.1	3.4
4	2	2	7.0	3.7	7.0	17.6	51.9	26.0	22.1	4	2	1.7
2	1	5	4.5	2.3	28.2	35.0	25.0	12.5	62.5	2	1	5
2	5	1	11.5	30.7	14.6	56.7	24.7	62.5	12.8	2.1	5.2	1.1
3	1	4	6.7	2.7	20.4	29.7	38.0	15.2	46.8	3	1.2	3.7
3	4	1	9.8	13.2	8.4	31.4	39.0	48.1	13.0	3	3.7	1
1	5	2	3.1	17.7	17.1	37.8	11.4	62.6	26.0	0.8	4.8	2
1	6	1	4.6	28.1	9.6	42.3	13.1	75.7	11.2	1	5.8	0.9
4	1	3	9.8	3.0	19.7	32.4	47.3	13.7	39.0	3.63	1.1	3
5	1	2	28.6	7.6	28.0	64.1	60.6	15.2	24.2	5.0	1.3	2.0
5	2	1	17.3	8.8	8.5	34.7	59.3	28.7	12.0	5	2.4	1
1	1	6	2.6	2.5	33.2	38.2	14.0	12.6	73.4	1.1	1	5.8
1	3	4	2.6	8.4	28.9	40.0	11.6	35.6	52.7	1	3	4.4
1	4	3	3.9	16.5	29.2	49.6	12.4	49.8	37.9	1.0	4.2	3.2
1	2	5	2.2	5.0	27.3	34.5	12.2	26.2	61.6	1	2.1	5
6	1	1	20.1	4.2	8.9	33.2	72.5	14.4	13.1	5.5	1.1	1
2	3	5	7.2	11.6	45.0	63.7	19.6	30.1	50.3	2.0	3.0	5.0
5	2	3	20.0	8.7	29.5	58.1	49.6	20.4	30.0	4.9	2.0	3.0
2	5	3	8.6	21.8	32.5	62.8	20.1	48.7	31.2	2.0	4.8	3.1
4	1	5	12.1	3.9	36.7	52.6	39.4	11.9	48.7	3.9	1.2	4.9
1	5	4	3.7	17.2	33.7	54.5	10.8	48.4	40.8	1.1	4.8	4.1
1	4	5	3.5	13.1	38.5	55.1	11.1	39.3	49.7	1.1	3.9	5.0
8	0	2	41.4	1.4	25.0	67.8	78.2	2.5	19.3	7.8	0.0	1.9
4	5	1	18.7	28.7	13.5	60.8	36.3	52.9	10.7	3.6	5.3	1.1
2	8	0	18.7	38.9	1.8	59.4	33.2	65.5	1.3	2.0	4.0	0.0
0	8	2	0.1	24.2	29.6	53.9	0.3	65.4	34.4	0.0	3.8	2.0
3	2	5	9.4	6.9	49.3	65.5	26.1	18.0	55.9	2.9	2.0	6.2
3	5	2	14.1	24.7	23.1	61.9	29.9	49.9	20.1	3.0	5.0	2.0
5	3	2	20.9	13.5	21.0	55.4	49.4	30.3	20.3	4.9	3.0	2.0
5	1	4	17.6	4.4	32.3	54.2	50.3	11.8	37.8	5.0	1.2	3.8
5	4	1	22.3	19.6	11.2	53.1	49.1	40.8	10.1	4.9	4.1	1.0
0	2	8	0.5	6.9	54.7	62.0	1.5	22.2	76.3	0.0	2.2	7.6
2	0	8	6.4	0.5	51.1	58.0	23.1	1.7	75.2	2.0	0.0	6.0
8	2	0	41.1	11.3	0.9	53.2	78.8	20.5	0.7	7.9	2.1	0.0
7	1	2	39.3	5.3	25.8	70.4	71.7	9.1	19.2	7.0	1.0	2.0
2	1	7	7.0	3.0	48.0	58.0	23.6	9.7	66.7	2.3	1.0	6.6

1	7	2	5.3	23.5	26.2	55.0	13.8	58.3	27.9	1.0	4.2	2.0
1	2	7	2.7	5.9	40.2	48.8	11.1	22.6	66.4	1.0	2.0	6.6
2	7	1	10.5	35.5	13.4	59.4	21.1	67.8	11.1	2.1	6.8	1.1
7	2	1	42.9	8.1	13.9	64.9	76.3	13.7	10.1	7.6	1.3	1.0
0	5	5	2.1	17.8	40.8	60.6	5.8	47.5	46.7	0.0	5.0	5.0
5	5	0	38.0	24.8	1.1	63.9	61.3	37.9	0.7	6.2	3.8	0.0
3	3	4	11.7	11.2	35.3	58.1	31.9	28.8	39.3	3.2	2.9	3.9
3	4	3	14.9	19.1	34.6	68.7	31.6	38.4	30.0	3.2	3.8	3.0
4	3	3	15.3	10.6	27.7	53.6	41.8	27.4	30.8	4.2	2.7	3.1
6	3	1	27.8	13.7	11.1	52.7	61.3	28.7	10.0	6.1	2.9	1.0
1	6	3	3.8	21.4	24.5	49.7	11.3	59.4	29.3	1.1	6.0	2.9
3	6	1	15.2	30.2	13.3	58.7	30.8	58.1	11.1	3.1	5.8	1.1
1	3	6	4.3	9.9	48.0	62.2	12.9	28.3	58.9	1.3	2.8	5.9
6	1	3	33.7	6.6	38.4	78.7	60.5	11.3	28.2	6.0	1.1	2.9
3	1	6	12.2	4.7	53.7	70.6	31.7	11.6	56.8	3.2	1.1	5.7

Table S1. (Supplementary Table 1) Inductively coupled plasma mass spectrometry (ICP-MS)

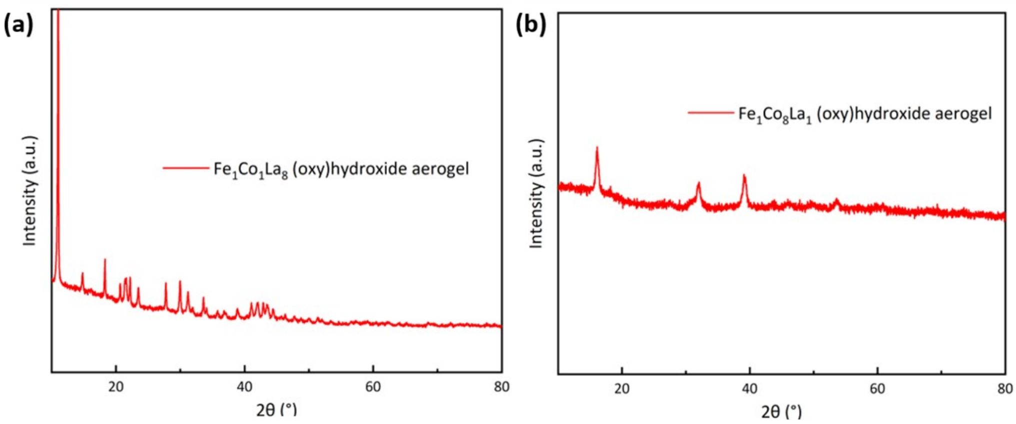

Figure S1. XRD pattern of the $Fe_xCo_yLa_z$ (oxy)hydroxide aerogel, diffraction peaks were observed once an element is significantly higher (x, y or z $\geq$ 8) than the other two.

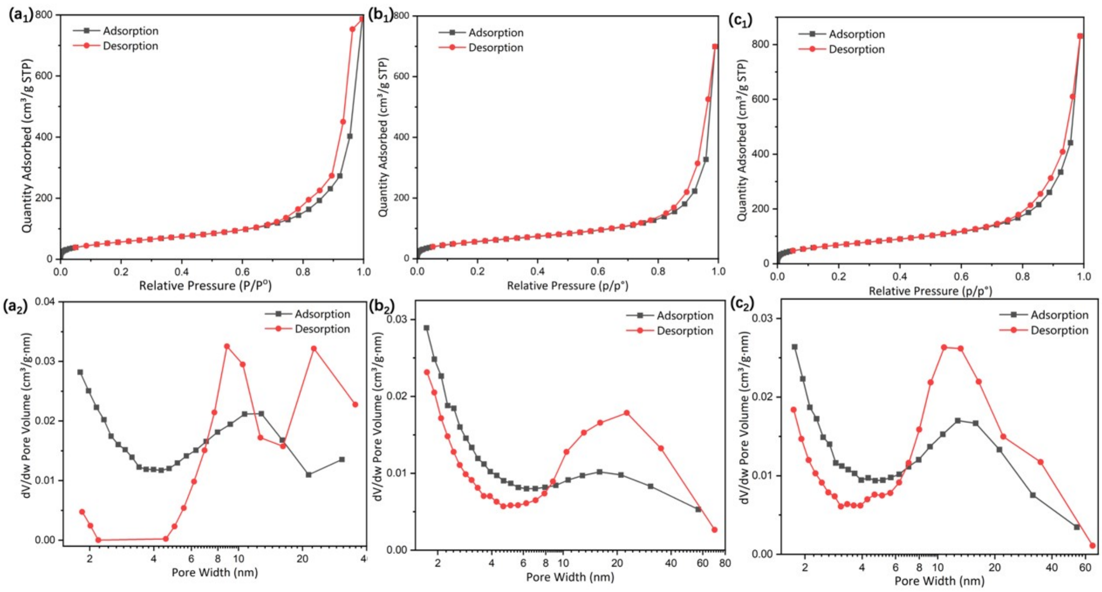

Figure S2. Isotherm linear plot of BET characterization results of **(a$_1$)** $Fe_4Co_4La_2$ (oxy)hydroxide aerogel, with BET surface area of 207.07 m^2 g^{-1}, **(a$_2$)** average pore size of ~15 nm; **(b$_1$)** Fe_4Co_6 (oxy)hydroxide aerogel, with a surface area of 251.94 m^2 g^{-1}, **(b$_2$)** average pore size of ~20 nm; **(c$_1$)** $Fe_3Co_3La_2$ (oxy)hydroxide aerogel, with BET surface area of 209.17 m^2 g^{-1}, **(c$_2$)** average pore size of ~20 nm.

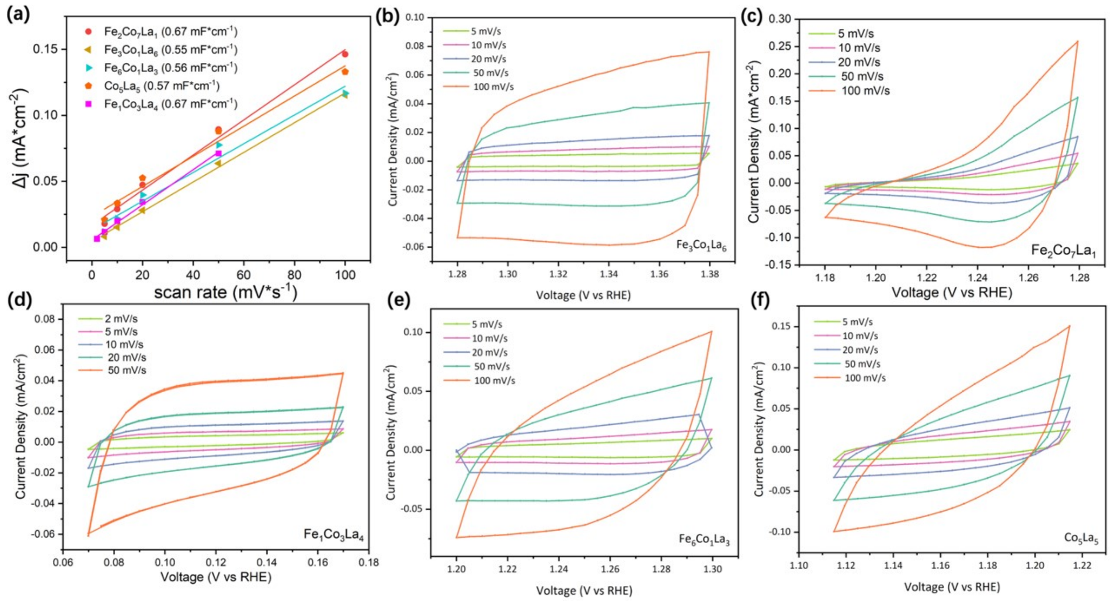

(g) Fe	Co	La	j_{250} (η=250mV VS Ref) (mA/cm2)	j_{350} (η=350mV VS Ref) (mA/cm2)	C_{dl}
6	1	3	6.1	49.6	0.55
3	1	6	5.6	61.9	0.56
1	3	4	18.5	95.8	0.67
0	5	5	5.3	47.7	0.57
2	7	1	36.1	120.0	0.67

Figure S3. (a) The corresponding C_{dl} derived from different scan rates via CV and **(b-f)** the electrochemical active surface area (ECSA) of selected samples. **(g)** A summary of the ECSA analysis of selected samples.

Element Ratio			Catalytic Performance			
Fe	Co	La	η_{onset} (mV)	η_{10} (mV)	η_{100} (mV)	Tafel Slope (mV dev^{-1})
2	3	3	216±6	227±6	337±6	40.03
2	4	2	199±8	210±6	315±8	44.39
3	3	2	260±3	290±2	460±3	48.28
3	2	3	221±2	226±3	335±3	36.49
4	2	2	226±5	236±0	364±5	42.58
2	1	5	255±4	270±3	400±3	40.62
2	2	4	233±3	240±3	360±6	39.77
2	5	1	216±5	230±11	353±13	45.19
3	1	4	240±3	280±4	460±6	41.25
3	4	1	220±8	232±6	354±11	42.92
1	5	2	210±6	216±8	322±8	59.32
1	6	1	215±11	219±2	331±6	50.66
4	1	3	244±4	254±5	383±3	37.6
5	1	2	238±5	244±8	379±8	35.82
5	2	1	260±4	290±1	420±4	46.08
1	1	6	285±2	306±3	460±2	41
1	3	4	219±2	234±4	357±3	43.67
1	4	3	220±8	230±9	339±12	48.07
4	2	1	213±3	220±5	334±4	41.32
1	2	5	249±4	259±2	375±9	43.27
6	1	1	265±10	286±3	461±14	42.09
2	3	5	240±15	250±19	430±27	45.48
5	2	3	226±13	238±14	378±18	36.14
2	5	3	209±5	215±9	319±9	43.17
4	1	5	244±3	252±5	380±6	35.71
1	5	4	226±3	233±5	350±3	51.75
1	4	5	252±3	260±3	372±3	43.14
8	0	2	354±2	386±5	692±1	41.78
4	5	1	207±8	222±9	340±8	43.1
2	8	0	230±3	240±3	390±5	49.27
0	8	2	220±4	250±6	430±4	57.64
3	2	5	231±5	240±5	338±11	38.18
3	5	2	208±5	220±6	346±9	47.67
5	3	2	218±5	229±7	345±5	38.94
5	1	4	244±9	264±9	429±12	35.95
5	4	1	220±8	230±16	350±8	43.21
0	2	8	280±3	340±8	630±9	56.92
2	0	8	335±2	487±5	700±5	53.82
8	2	0	250±5	260±6	430±14	47.17
7	1	2	251±5	260±3	395±5	37.33

2	1	7	249±2	255±1	366±6	36.92
1	7	2	214±11	225±12	342±11	48.17
1	2	7	266±3	278±3	408±3	40.14
2	7	1	202±3	208±3	327±5	54.16
7	2	1	230±5	240±6	369±14	39.93
0	5	5	250±6	270±3	420±9	62.66
5	5	0	202±3	213±1	338±3	49.93
3	3	4	223±3	230±3	334±4	36.3
3	4	3	234±11	239±6	334±5	36.3
1	1	8	266±4	279±5	425±4	38.27
4	3	3	224±2	237±3	363±4	43.97
4	4	2	223±4	237±5	370±8	39.14
4	6	0	196±6	204±9	326±12	52.8
8	1	1	235±3	251±3	417±7	35.33
9	1	0	327±5	347±3	534±0	52
0	1	9	300±2	433±5	700±5	49.96
1	0	9	204±8	213±7	345±8	57.3
1	8	1	241±3	248±3	362±3	38.22
2	2	6	233±3	239±2	350±3	39.92
2	4	4	201±5	209±5	319±5	49.86
2	6	2	221±3	228±3	338±4	35.95
4	2	4	239±3	246±3	384±5	36.65
6	2	2	189±4	204±2	342±3	47.36
6	4	0	233±3	245±3	419±5	33
9	1	0	221±2	231±4	350±5	43.39
6	3	1	229±8	239±10	356±12	49.58
1	6	3	221±8	226±9	361±8	44.88
3	6	1	263±3	274±3	400±5	44.38
1	3	6	247±17	266±21	449±7	33.14
6	1	3	249±10	263±9	402±15	33.42
3	1	6	283±6	297±3	434±6	51.57
0	3	7	191±3	209±1	354±2	50.71
3	7	0	212±5	230±3	407±18	42.58
7	3	0	260±8	283±1	450±3	39.57
7	0	3	249±2	255±1	366±6	36.92

Table S2. Summary of the stoichiometries study on the electrochemical properties for the selected combinatorial catalysis system: $Fe_xCo_yLa_z$ (oxy)hydroxide aerogel.

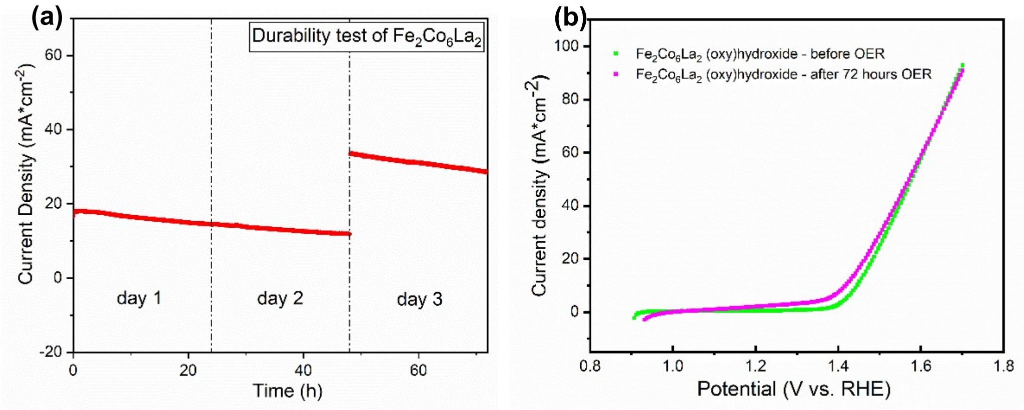

Figure S4. (a) Durability test of $Fe_2Co_6La_2$-based amorphous aerogel sample at current densities of 20 mAcm-2 and 30 mAcm-2 for 72 hour; **(b)** linear sweep voltammetries before and after 72 hours' stability test.

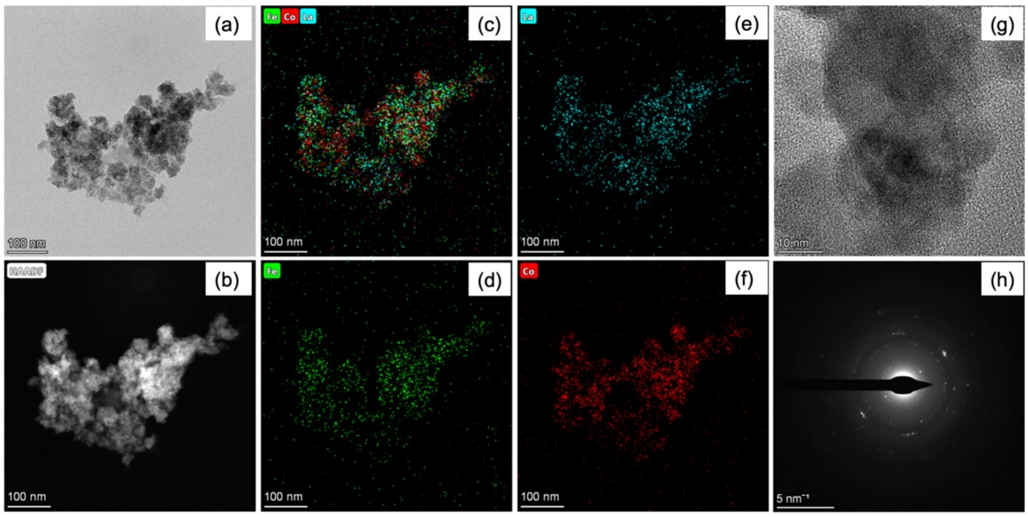

Figure S5. Characterization of $Fe_2Co_6La_2$ (oxy)hydroxide aerogels after OER **(a,b)** TEM and HAADF images; **(c, d, e and f)** EDS mapping; **(g)** HRTEM; **(h)** the SAED.

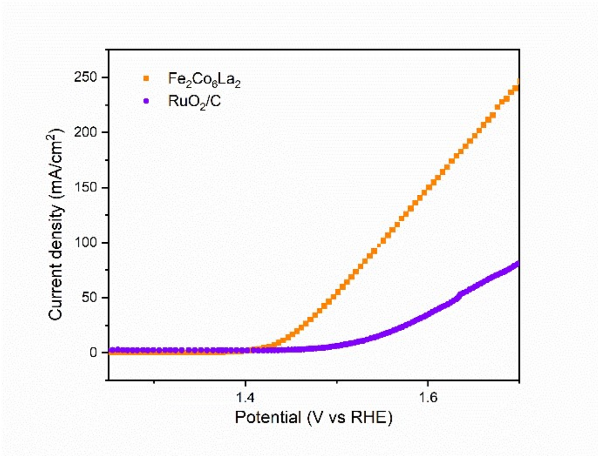

Figure S6. Electrocatalytic properties and Mass Productivity of aerogels with selected compositions and commercial catalysts. (LSV plot without iR compensation)

Notes: Mass activity is calculated by:

$$Mass\ activity = \frac{Current\ at\ at\ 1.67V\ (RHE)\ (mA)}{Metal\ loading\ on\ GCE\ (mg)} = \frac{Current\ density\ at\ 1.67V\ (RHE)\ mA\ cm^2 * 0.0707\ cm^2}{Metal\ loading\ on\ GCE\ (mg)}$$

Metal loading of catalysis was measured by the ICP-OES, $Fe_{20}Co_{60}La_{20}$ (oxy)hydroxides-gel, which showed a similar value around 60 wt%. Metal loading on GCE (mg) = 60 wt% * 5 mg * (5 ul / 1100 ul). The mass loading of RuO_2 catalyst is 0.025 mg cm^{-2}, which were provided by previous works,[28] and have been verified.

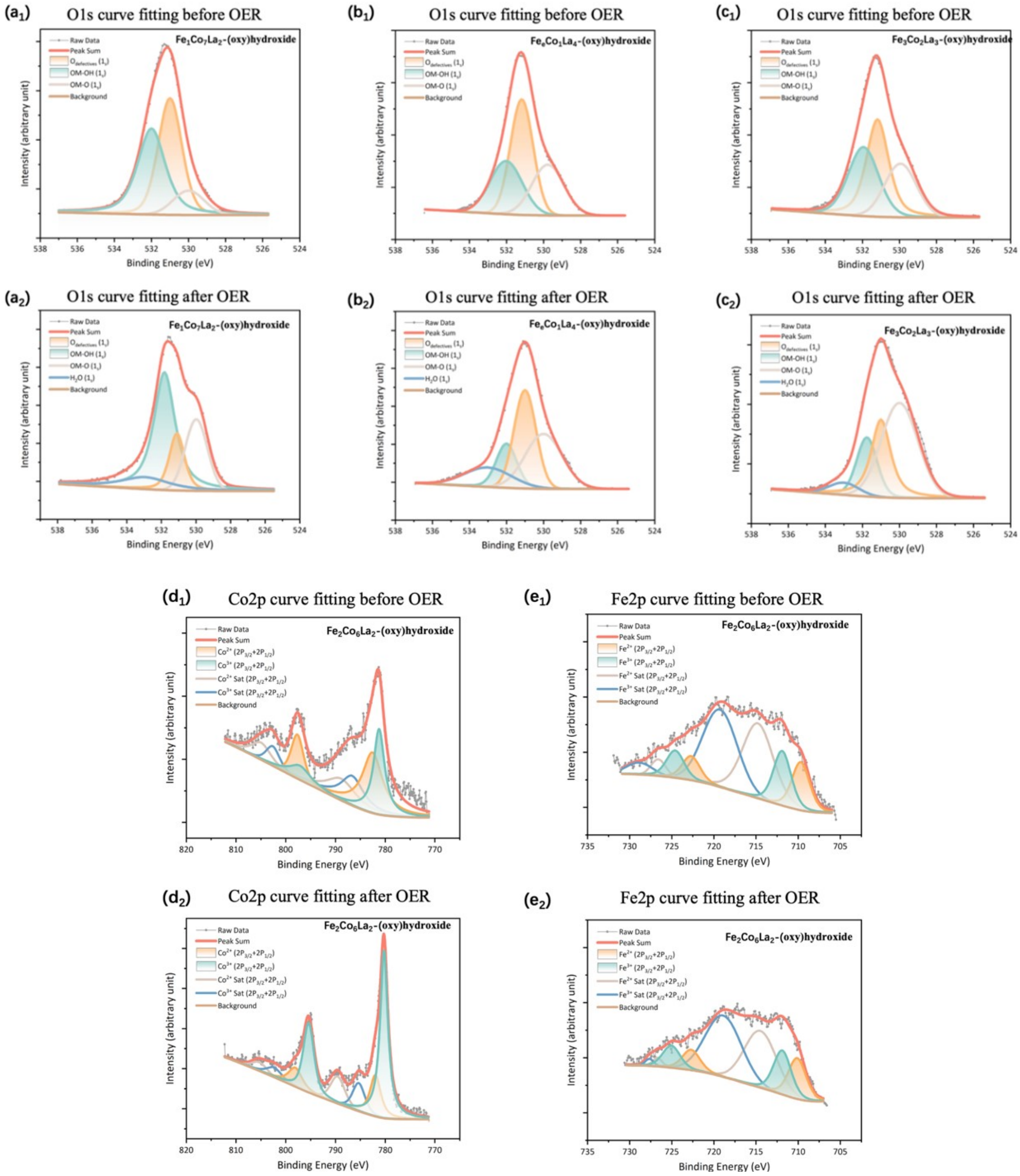

Figure S7. A few examples of X-ray photoelectron spectroscopy studies on selected aerogels. **(a_{1-2})** The XPS high-resolution spectrum of O 1s showed four peaks at around 530 eV, 531 eV, 532 eV and 534 eV which can be assigned to metal oxide (O_{M-O}), defective oxygen sites ($O_{Defective}$), hydroxide (O_{M-OH}), and adsorbed H_2O ($H_2O_{adsorbed}$) respectively. $Fe_xCo_yLa_z$ aerogel are examined to be mostly consisted with (oxy)hydroxide ($O_{Defective}$ and O_{M-OH}), after OER the content of metal oxide(O_{M-O}) increase.[2–6] The XPS high-resolution spectrum of Co 2p showed peaks at: ca.782.4 eV, 798 eV are assigned to Co^{2+} in Co $2p_{3/2}$ and Co $2p_{1/2}$; ca.780.5 eV, 796 eV are assigned to Co^{3+} in Co $2p_{3/2}$ and Co $2p_{1/2}$; 789 eV and 805 eV are assigned to Co^{2+} satellite peaks;

786 eV and 802 eV are assigned to Co^{3+} satellite peaks.[7–9] The peaks located at ca.709.7 eV, 723.4 eV are assigned to Fe^{2+} in Fe $2p_{3/2}$ and Fe $2p_{1/2}$; ca.709.7 eV, 723.4 eV are assigned to Fe^{3+} in Fe $2p_{3/2}$ and Fe $2p_{1/2}$; 716 eV and 727 eV are assigned to Fe^{2+} satellite peaks, and 718 eV and 729 eV are assigned to Fe^{3+} satellite peaks.[10–12]

(a) XPS analysis of O 1s before 100 times of cyclic voltammetry

$Fe_xCo_yLa_z$	O^{2-}		O_{vac}		O_{OH-}		O_{H2O}		O^{2-}	O_{vac}	O_{OH-}
	B.E. (eV)	area	B.E. (eV)	area	B.E. (eV)	area	B.E. (eV)	area	(%)	(%)	(%)
172	530.0	10394	531.0	41930	532.0	41642	-	-	0.11	0.45	0.44
271	530.0	37966	531.0	34745	532.0	15730	-	-	0.43	0.39	0.18
280	530.0	31536	531.2	24938	531.9	34829	-	-	0.35	0.27	0.38
325	530.0	23744	531.0	34119	532.0	12201	-	-	0.34	0.49	0.17
415	530.0	41393	531.0	26439	532.0	16971	-	-	0.49	0.31	0.20
433	530.0	34284	531.0	34356	532.0	17803	-	-	0.40	0.40	0.21
505	530.0	22004	531.0	25091	532.0	19267	-	-	0.33	0.38	0.29
523	530.0	44577	531.0	24925	532.0	13380	-	-	0.54	0.30	0.16
532	530.0	40337	531.0	36870	532.0	17318	-	-	0.43	0.39	0.18
631	530.0	34329	531.0	29991	532.0	17283	-	-	0.42	0.37	0.21
712	530.0	31375	531.0	36582	532.0	22357	-	-	0.35	0.41	0.25
721	530.0	38273	531.0	39604	532.0	17385	-	-	0.40	0.42	0.18
224	530.0	21342	531.0	37723	532.0	19670	-	-	0.27	0.48	0.25
314	530.0	21067	531.0	33875	532.0	22288	-	-	0.27	0.44	0.29
323	530.0	22148	531.0	34905	532.0	29061	-	-	0.26	0.41	0.34
208	530.2	4806	532.0	15353	532.9	8910	-	-	0.17	0.53	0.31
262	530.4	4554	531.7	27771	532.7	20365	-	-	0.09	0.53	0.39
316	530.0	3992	531.3	56016	532.1	42327	-	-	0.04	0.55	0.41
424	530.5	4802	532.0	38843	532.9	27259	-	-	0.07	0.55	0.38
613	529.6	26792	530.9	47230	531.8	23459	-	-	0.27	0.48	0.24
640	530.1	9308	531.7	21538	532.7	11008	-	-	0.22	0.51	0.26
910	530.4	44738	531.1	52402	532.0	15585	-	-	0.40	0.46	0.14

(b) XPS analysis of O 1s after 100 times of cyclic voltammetry

$Fe_xCo_yLa_z$	O^{2-}		O_{vac}		O_{OH-}		O_{H2O}		O^{2-}	O_{vac}	O_{OH-}	O_{H2O}
	B.E. (eV)	area	B.E. (eV)	area	B.E. (eV)	area	B.E. (eV)	area	(%)	(%)	(%)	(%)
172	530.0	15024	531.0	10225	532.0	33210	533.0	7850	0.23	0.15	0.50	0.12
271	530.0	16921	531.0	21056	532.0	12811	533.0	12165	0.27	0.33	0.20	0.19
280	530.0	10551	531.0	12031	532.0	18590	533.0	11248	0.20	0.23	0.35	0.21
325	530.0	20590	531.0	29557	532.0	15495	533.0	6823	0.28	0.41	0.21	0.09
415	530.0	37736	531.0	17471	532.0	8615	533.0	4192	0.55	0.26	0.13	0.06
433	530.0	38121	531.0	19119	532.0	8340	533.0	5080	0.54	0.27	0.12	0.07
505	530.0	51757	531.0	19248	532.0	8990	533.0	6527	0.60	0.22	0.10	0.08
523	530.0	29619	531.0	19651	532.0	10898	533.0	10774	0.42	0.28	0.15	0.15
532	530.0	16452	531.0	17419	532.0	6409	533.0	6111	0.35	0.38	0.14	0.13
631	530.0	19450	531.0	14463	532.0	16667	533.0	6639	0.34	0.25	0.29	0.12
712	530.0	16809	531.0	14596	532.0	8388	533.0	7945	0.35	0.31	0.18	0.17

721	530.0	13801	531.0	10610	532.0	9394	533.0	6319	0.34	0.26	0.23	0.16
224	530.0	19364	531.0	22013	532.0	9944	533.0	6725	0.33	0.38	0.17	0.12
314	530.0	18110	531.0	19223	532.0	8680	533.0	8213	0.33	0.35	0.16	0.15
323	530.0	39544	531.0	23276	532.0	14738	533.0	4142	0.48	0.28	0.18	0.05
208	529.7	8244	531.3	18492	532.3	11018	535.1	9060	0.18	0.40	0.24	0.19
262	530.2	17378	531.5	31313	532.4	14103	535.1	6737	0.25	0.45	0.20	0.10
316	530.4	39718	531.2	45134	532.2	18577	535.0	563	0.38	0.43	0.18	0.01
424	530.1	19122	531.5	46516	532.5	28292	535.3	5895	0.19	0.47	0.28	0.06
613	529.6	40251	530.8	38258	531.8	19321	533.0	2951	0.40	0.38	0.19	0.03
640	529.7	13186	531.2	27809	532.2	10839	535.0	6396	0.23	0.48	0.19	0.11
910	530.0	32273	531.3	48418	532.2	18565	538.3	6113	0.31	0.46	0.18	0.06

(c) XPS analysis of Co 2p before 100 times of cyclic voltammetry

$Fe_xCo_yLa_z$	Co^{2+} ($2p_{3/2}$)		Co^{2+} ($2p_{1/2}$)		Co^{3+} ($2p_{3/2}$)		Co^{3+} ($2p_{3/2}$)		Co^{2+} (%)
	B.E. (eV)	**area**	**B.E. (eV)**	**area**	**B.E. (eV)**	**area**	**B.E. (eV)**	**area**	
172	782.19	41950.21	797.72	21781.13	780.69	29541.21	796.44	18940.72	0.57
271	782.37	48888.59	797.55	46656.01	780.48	47575.68	796.24	28128.56	0.56
280	782.25	56793.39	797.71	27717.28	780.67	36534.64	796.35	28849.60	0.56
325	782.39	18895.24	797.94	5454.95	780.62	20269.11	796.08	9493.22	0.45
415	782.42	13165.94	798.30	2311.38	780.47	16153.54	795.73	7905.51	0.39
433	782.4	16261.18	798	7115.18	780.5	19106	796	9941.78	0.45
523	782.64	14849.08	797.40	5074.48	780.20	16602.96	795.71	9156.07	0.44
532	782.49	24075.85	797.34	9860.97	780.42	22848.08	795.75	14068.94	0.48
631	782.49	26682.25	797.53	10167.39	780.54	26503.67	796.02	16622.94	0.46
712	782.27	30653.26	797.68	13387.74	780.62	24793.70	796.31	18978.72	0.50
721	782.40	18219.13	798.00	4995.02	780.50	19788.88	796.00	12082.41	0.42
224	782.45	19766.67	797.62	10106.80	780.50	20422.86	796.24	11528.08	0.48
314	782.40	14719.70	798.00	6545.29	780.50	18079.90	796.00	8287.10	0.45
323	782.34	18267.80	797.81	5881.46	780.80	13670.38	796.48	6912.43	0.54
262	782.56	14858.37	797.66	5451.88	781.24	11408.62	797.12	3688.48	0.57
316	782.40	4151.77	798.00	964.47	780.50	7483.23	796.00	2961.36	0.33
424	782.40	4851.63	796.83	2212.33	780.50	5837.61	796.00	2251.40	0.47
613	782.11	8958	796.27	2172.99	779.9	12654.8	794.56	3989.39	0.40
640	782.53	10058.81	798.06	5313.52	780.80	7648.05	796.20	2905.20	0.59
910	782.48	71539.63	797.62	32073.13	780.43	76519.38	796.19	39876.89	0.47

(d) XPS analysis of Co 2p after 100 times of cyclic voltammetry

$Fe_xCo_yLa_z$	Co^{2+} ($2p_{3/2}$)		Co^{2+} ($2p_{1/2}$)		Co^{3+} ($2p_{3/2}$)		Co^{3+} ($2p_{3/2}$)		Co^{2+} (%)
	B.E. (eV)	**area**	**B.E. (eV)**	**area**	**B.E. (eV)**	**area**	**B.E. (eV)**	**area**	
172	782.17	21089.03	798.15	9331.73	780.51	33615.65	795.73	23689.09	0.35
271	782.21	31448.88	798.14	14677.14	780.50	41611.87	795.75	33116.54	0.38
280	782.10	21811.80	798.00	10139.99	780.62	21740.63	795.93	17724.23	0.45
325	782.4	12553.3	796.95	6358.82	780.5	19601.44	795.43	8478.81	0.40

415	782.68	5609.51	797.31	875.40	780.16	8690.04	795.77	4844.97	0.32
433	782.90	16268.67	798.21	9749.15	780.12	43888.83	795.24	26346.38	0.27
523	782.59	8268.23	798.25	3180.74	780.25	16126.38	795.51	9261.79	0.31
532	782.75	12682.60	797.60	8033.57	780.28	30395.71	795.32	16473.07	0.31
631	782.27	19079.51	797.66	7062.04	780.48	26706.93	795.67	17081.28	0.37
712	782.40	6780.34	798.47	2356.24	780.44	7505.74	795.61	5271.40	0.42
721	782.58	5750.77	798.13	2819.51	780.26	11766.35	795.41	7223.38	0.31
224	781.55	7281.10	798.71	3401.31	780.54	16732.98	795.63	9073.35	0.29
314	782.40	4438.36	796.77	2646.25	780.50	9801.56	795.20	3875.91	0.34
323	782.54	14919.23	797.75	5968.61	780.24	32906.90	795.31	17524.31	0.29
262	781.97	7926.95	798.07	4494.24	780.26	24590.68	795.40	12012.48	0.25
316	782.40	2569.23	798.00	1499.68	780.50	11800.68	796.00	4340.16	0.20
424	782.73	12553.52	798.19	8025.64	780.24	36427.63	795.37	21893.95	0.26
613	782.76	9257.32	797.41	2184.35	780.03	15374.86	795.27	8120.04	0.33
640	782.35	11063.78	798.36	5282.65	780.12	20188.60	795.22	14651.04	0.32
910	782.28	43676.25	798.28	12388.99	780.42	74190.22	795.60	54232.19	0.30

(e) XPS analysis of Fe 2p before 100 times of cyclic voltammetry

$Fe_xCo_yLa_z$	Fe^{2+} ($2p_{3/2}$)		Fe^{2+} ($2p_{1/2}$)		Fe^{3+} ($2p_{3/2}$)		Fe^{3+} ($2p_{31/2}$)		Fe^{2+} (%)
	B.E. (eV)	area	B.E. (eV)	area	B.E. (eV)	area	B.E. (eV)	area	
172	710.18	7443.93	723.06	2058.69	712.00	9446.49	724.93	3513.88	0.42
271	709.82	10329.26	723.00	3965.48	711.55	11053.39	724.41	4137.83	0.48
280	710.25	14068.43	723.05	6334.22	711.81	18874.91	724.83	8224.71	0.43
325	782.39	18895.24	797.94	5454.95	780.62	20269.11	796.08	9493.22	0.45
415	782.42	13165.94	798.30	2311.38	780.47	16153.54	795.73	7905.51	0.39
433	782.40	18726.38	797.51	9746.79	780.43	19243.70	796.05	12309.32	0.47
505	710.34	11366.01	723.41	5160.17	711.78	14063.40	724.88	6595.73	0.44
523	709.87	15061.45	723.16	7154.19	711.54	14623.42	724.81	6907.87	0.51
532	709.98	15119.55	723.14	6702.75	711.58	19166.69	724.71	8795.84	0.44
631	710.04	13438.39	723.18	6341.50	711.48	21052.19	724.78	10526.09	0.39
712	710.12	14251.40	723.21	6413.13	711.65	19359.16	724.80	7926.04	0.43
721	710.04	27834.72	723.16	12694.43	711.74	21629.13	724.77	9317.10	0.57
224	710.11	7038.58	723.00	3519.29	711.74	8805.60	724.70	4402.80	0.44
314	710.00	8097.84	723.28	3553.89	711.44	8674.09	724.60	3820.29	0.48
323	710.11	9121.14	723.18	3874.66	711.59	14254.69	724.80	7040.99	0.38
208	709.66	5648.96	722.50	3067.44	711.50	6134.89	724.49	3067.44	0.49
262	709.69	5327.58	722.70	2663.79	711.89	6022.56	724.59	3011.28	0.47
316	710.00	2830.89	722.70	1415.44	711.82	4801.77	725.00	2400.88	0.37
424	711.02	5666.37	722.70	2833.19	712.62	3102.94	724.50	1551.47	0.65
613	709.70	11846.42	723.24	5618.60	711.22	12174.99	724.92	6186.61	0.49
640	710.13	7266.00	723.12	2622.29	711.82	9238.72	724.51	3254.98	0.44
910	710.69	18030.22	721.38	6011.54	712.54	17988.49	724.27	8994.24	0.47

(f) XPS analysis of Fe 2p after 100 times of cyclic voltammetry

$Fe_xCo_yLa_z$	Fe^{2+} (2p3)		Fe^{2+} (2p1)		Fe^{3+} (2p3)		Fe^{3+} (2p1)		Fe^{2+} (%)
	B.E. (eV)	area	B.E. (eV)	area	B.E. (eV)	area	B.E. (eV)	area	
172	710.16	1861.11	722.70	739.85	711.15	2472.92	724.50	912.58	0.43
271	709.93	2808.84	723.00	852.90	711.50	4913.63	724.30	1247.59	0.37
280	710.37	3052.79	722.96	1013.75	711.50	4945.51	724.50	1900.93	0.37
325	710.00	4600.02	722.79	2300.01	711.42	7748.86	724.40	3874.43	0.37
415	709.67	8016.01	723.07	3426.49	711.08	9231.36	724.25	4262.12	0.46
433	709.75	5931.77	722.90	2669.30	711.26	6177.18	724.30	2501.76	0.50
505	709.90	12002.90	723.12	5401.31	711.17	16045.36	724.48	7220.41	0.43
523	709.85	6897.95	723.26	3104.08	711.17	8021.69	724.50	3333.51	0.47
532	709.72	3249.63	722.90	1299.85	711.46	4887.47	724.40	1954.99	0.40
631	710.11	6622.97	722.87	3012.11	711.48	7437.58	724.46	3346.91	0.47
712	709.93	6244.42	723.38	2584.29	711.35	9007.96	724.74	3550.70	0.41
721	709.82	5683.59	723.03	1127.09	711.63	6175.24	724.34	1646.67	0.47
224	709.88	2677.64	722.91	1071.06	711.37	4034.02	724.40	1815.31	0.39
314	709.80	2508.64	722.72	1254.32	711.10	3574.92	724.50	1787.46	0.41
323	709.73	7011.29	722.97	3211.17	711.16	9956.00	724.45	4490.61	0.41
208	710.04	8711.51	722.00	3605.01	712.00	7210.01	724.57	3605.01	0.53
262	710.11	4506.37	722.70	2253.19	711.88	4856.16	725.05	2406.60	0.48
316	710.26	5455.68	722.55	1954.18	712.11	4448.02	724.99	2714.25	0.51
424	710.18	5478.86	722.70	2739.43	711.88	6871.96	724.90	3435.98	0.44
613	709.84	15321.59	723.15	7660.79	711.31	18933.92	724.90	9466.96	0.45
640	710.05	7158.83	723.00	2033.78	711.73	8169.09	724.40	2730.73	0.46
910	710.52	11615.31	722.00	6361.41	712.50	14221.02	724.78	5985.95	0.47

Table S3. X-ray photoelectron spectroscopy studies on selected aerogels before and after OER. Peaks information for XPS high-resolution spectra after curve fitting: **(a-b)** O 1s, **(c-d)** Co 2p and **(e-f)** Fe 2p.

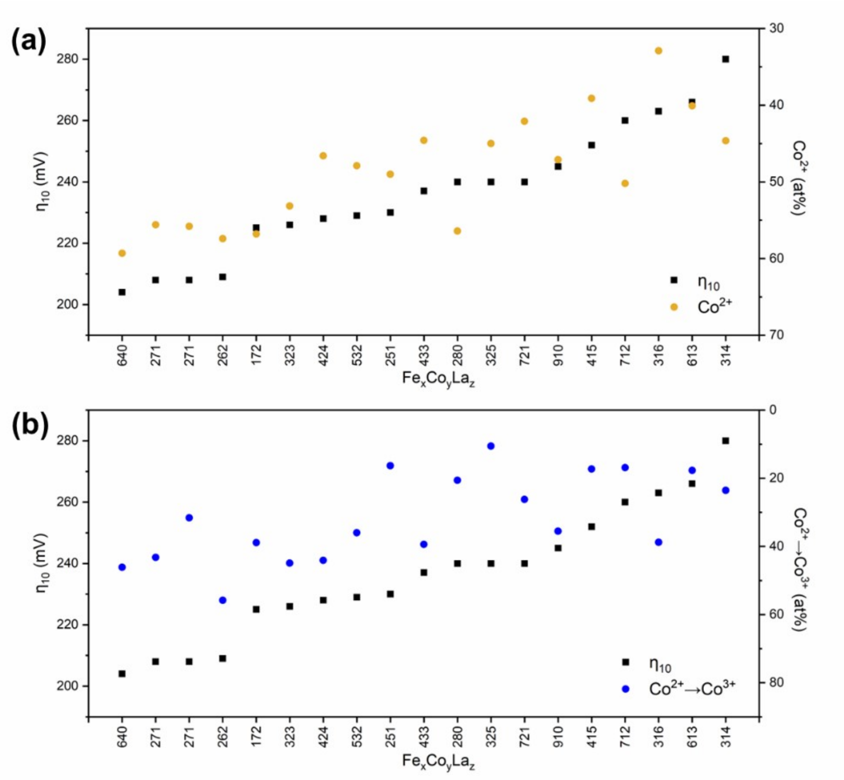

Figure S8. The demonstration of the corresponding relationship between **(a)** the ratio of Co^{2+} in (Co^{2+} + Co^{3+}) before the OER reaction, **(b)** the conversion of Co^{2+} to Co^{3+} after the reaction within selected aerogel samples and their catalytic performance (η_{10}).

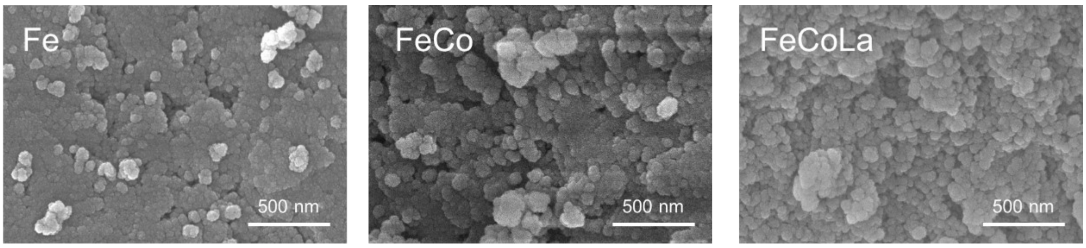

Figure S9. SEM images of binary aerogel and Ternary aerogels

	Bond	**R(Å)**	**CN**	**R-factor**	**Sigma^2**	**E_0 (eV)**	**ΔR**
Fe_3O_2- aerogel	Co-O	2.03	5.7	0.007	0.01	-2.29	-0.54
	Fe-O	1.97	5.9	0.005	0.01	-1.06	0.037
Fe_3Co_3La-aerogel	Co-O	2.04	6	0.012	0.009	-1.40	-0.55
	Fe-O	1.98	5.88	0.006	0.01	-0.49	0.047

R is the bond length; CN is the coordination numbers; sigma^2 is the Debye-Waller factor.

Table S4. The fitting parameters of the Co and Fe k-edge EXAFS data

The Fourier Transform of the Co and Fe k-edge extended X-ray absorption fine structure (EXAFS) spectra of the Fe_3O_2-based aerogel and Fe_3Co_3La-based aerogel was carried out in Artemis (Version 0.9.26). The model of bulk Co, bulk Fe, CoOOH and FeOOH were used to calculate the simulated scattering paths. The fitted bond length (R), coordination numbers (CN), R-factors, sigma^2, E_0 and ΔR are summarized in **Table S4**.

References

1 K. Yang, P. Xu, Z. Lin, Y. Yang, P. Jiang, C. Wang, S. Liu, S. Gong, L. Hu and Q. Chen, *Small*, 2018, **14**, 1803009.

2 X. Bai, Y. Fan, C. Hou, T. Tang and J. Guan, *International Journal of Hydrogen Energy*, 2022, **47**, 16711–16718.

3 Z. Ye, C. Qin, G. Ma, X. Peng, T. Li, D. Li and Z. Jin, *ACS Applied Materials and Interfaces*, 2018, **10**, 39809–39818.

4 Y. Li, M. Lu, Y. Wu, Q. Ji, H. Xu, J. Gao, G. Qian and Q. Zhang, *Journal of Materials Chemistry A*, 2020, **8**, 18215–18219.

5 C. Dong, X. Yuan, X. Wang, X. Liu, W. Dong, R. Wang, Y. Duan and F. Huang, *Journal of Materials Chemistry A*, 2016, **4**, 11292–11298.

6 Y. Fu, L. Li, S. Ye, P. Yang, P. Liao, X. Ren, C. He, Q. Zhang and J. Liu, *Journal of Materials Chemistry A*, 2021, **9**, 453–462.

7 L. Tian, J. L. Zhu, L. Chen, B. An, Q. Q. Liu and K. L. Huang, *Journal of Nanoparticle Research*, 2011, **13**, 3483–3488.

8 J. Chen, H. Li, S. Chen, J. Fei, C. Liu, Z. Yu, K. Shin, Z. Liu, L. Song, G. Henkelman, L. Wei and Y. Chen, *Advanced Energy Materials*, 2021, **11**, 1–9.

9 F. T. Haase, A. Bergmann, T. E. Jones, J. Timoshenko, A. Herzog, H. S. Jeon, C. Rettenmaier and B. R. Cuenya, *Nature Energy*, 2022, **7**, 765–773.

10 N. S. McIntyre and D. G. Zetaruk, *Analytical Chemistry*, 1977, **49**, 1521–1529.

11 B. J. Tan, K. J. Klabunde and P. M. A. Sherwood, *Chemistry of Materials*, 1990, **2**, 186–191.

12 E. Chmielewská, W. Tylus, M. Drábik, J. Majzlan, J. Kravčak, C. Williams, M. Čaplovičová, and Čaplovič, *Microporous and Mesoporous Materials*, 2017, **248**, 222–233.